Received: 16 October 2025 | Revised: 24 February 2026 | Accepted: 28 April 2026 | Published online: 8 May 2026

RESEARCH ARTICLE

Journal of Optics and Photonics Research
2026, Vol. 00(00) 1–10
DOI: 10.47852/bonviewJOPR62027912

BON VIEW PUBLISHING

Scaling Rules for TM Modes in Thin–Film Optical Waveguides

Štefan Višňovský[1,*]

[1] *Faculty of Mathematics and Physics, Charles University, Czechia*

Abstract: Three-media planar dielectric nonmagnetic optical waveguides represent basic structures employed in integrated optics and sensing. The previously published scaling rules for transverse electric (TE) and transverse magnetic (TM) modes in these structures were characterized with different sets of parameters for TE and TM cases. The latter case which is more involved received less attention. The present work suggests an alternative approach where both TE and TM modes are characterized by the same set of three parameters, that is, normalized frequency or film thickness, normalized guide index, and asymmetry measure. A complete specification of the TM modes requires an additional parameter, that is, the ratio of the index of refraction in the film to that in the substrate. The TE and TM solutions for the normalized guide index and the normalized guide thickness are displayed in common charts as functions of normalized frequency. This provides an improved insight into the differences between the TE and TM guided modes.

Keywords: optical thin–film waveguides, transverse magnetic modes, normalized guide index, normalized effective film thickness, scaling rules

1. Introduction

Three-media planar dielectric optical waveguides represent basic structures employed in integrated optics and sensing [1–4]. Kogelnik and Ramaswamy developed the scaling rules for these structures [5]. The waveguiding conditions for transverse electric (TE) modes were represented in a simple and concise way thanks to negligible deviations of magnetic permeability from its vacuum value at optical frequencies [6]. To solve the more involved transverse magnetic (TM) case, Kogelnik and Ramaswamy [5] employed the parameters modified with respect to those employed in the TE case. Hewak and Lit [7, 8] proposed alternative parameters for the guided TM modes that are still different from those for the guided TE modes.

In the present work, we follow the work by Kogelnik and Ramaswamy [5] and propose to replace their treatment of the TM modes with the characteristics using the same set of normalized parameters for both guided TE and TM modes, that is, normalized frequency or film thickness (V), normalized guide index (b), and asymmetry measure (a). The present approach allows to compare the TE and TM guided modes in asymmetric slab waveguides and display them in common $b(V)$ charts. The normalized characteristics for TE and TM modes developed by Wang et al. [9] and applied in their studies of waveguides on left-handed materials are used.

In the following Section 2, we summarize the analysis of the three-media asymmetric planar dielectric nonmagnetic optical waveguide [5, 9–11]. We make use of the symmetry between TE and TM modes. This allows us to express the corresponding equations in a concise and transparent way. We list the dispersion equations deduced from Maxwell equations and boundary conditions at the film interfaces and related parameters, that is, lateral shifts (Goos–Hänchen shift), penetration depths of the rays internally reflected at interfaces, effective guide thickness, and the power carried by guided modes. The normalized dispersion equations and the equations for normalized effective guide thickness are applied in the construction of charts for the effective guide index and effective guide thickness in Sections 3 and 4. The paper is summarized in Section 5.

2. Asymmetric Planar Waveguide

2.1. Maxwell equations and boundary conditions

The basic model for the guided waves in planar dielectric waveguides considers a planar layered structure consisting of a film (1) sandwiched between semi-infinite media, a substrate (2), and a cover (3) [10, 12–14].

The film thickness, h, is defined as the distance between the parallel planes formed by the interface between (1) and (2) and that between (1) and (3). All three media are assumed uniform, isotropic, and linear. Each medium is characterized by the real electric permittivity ε_i and real magnetic permeability μ_i, $i = 1, 2,$ and 3 (Figure 1). The electric and magnetic fields of time (t) harmonic waves of the angular frequency ω can be found from the Maxwell equations:

$$\nabla \times \mathbf{E} = -\mathrm{j}\omega\mu\,\mathbf{H},\ \nabla \times \mathbf{H} = \mathrm{j}\omega\varepsilon\,\mathbf{E}, \tag{1}$$

***Corresponding author:** Štefan Višňovský, Faculty of Mathematics and Physics, Charles University, Czechia. Email: stefan.visnovsky@matfyz.cuni.cz

Figure 1
Asymmetric planar waveguide

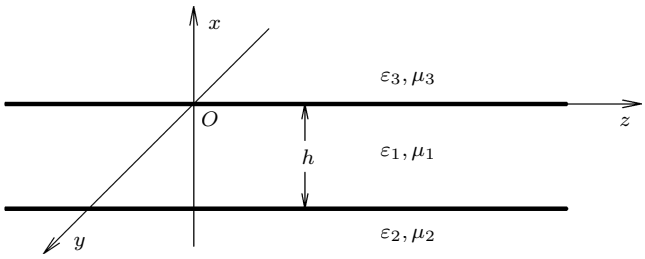

where $\omega = kc$ is related to the vacuum propagation constant, k, and wave phase velocity in a vacuum, c. The vacuum propagation constant, k is related to the vacuum wavelength, λ_{vac} as $k = 2\pi/\lambda_{\text{vac}}$.

Equation (1) satisfies the duality transformation, which requires the simultaneous exchange of electric, **E**, and magnetic, **H**, field vectors according to $\mathbf{E} \rightarrow \pm\mathbf{H}$, $\mathbf{H} \rightarrow \mp\mathbf{E}$, and $\varepsilon \leftrightarrow \mu$. For the t dependent guided waves propagating parallel to the z-axis, the **E**, and **H** fields are assumed proportional to $\exp[\mathrm{j}(\omega t - Nkz)]$. The propagation constant z component, Nk, is expressed as a product of k and the effective guide index, N. With the choice of interfaces in the planar layered structure normal to the x-axis, $\partial/\partial y = 0$. Then the solutions of the Maxwell equations can be separated into the TE (transverse electric) modes formed by the Cartesian field components E_y, H_x and H_z and into the TM modes formed by H_y, E_x and E_z [12].

The TE electric fields, $E_y^{(i)}$, in the three regions ($i = 1, \ldots, 3$), can be taken in the form [13]

$$\begin{aligned} E_y^{(3)} &= A\ \exp\left[-k\left(N^2 - n_3^2\right)^{1/2} x\right],\ x \geq 0, \\ E_y^{(1)} &= A\ \cos\left[k\left(n_1^2 - N^2\right)^{1/2} x\right] + B \sin\left[k(n_1^2 - N^2)^{1/2} x\right] \\ &\quad 0 \geq x \geq -h, \\ E_y^{(2)} &= \left\{A \cos\left[k\left(n_1^2 - N^2\right)^{1/2} h\right] - B \sin\left[k(n_1^2 - N^2)^{1/2} h\right]\right\} \\ &\quad \times \exp\left[k\left(N^2 - n_2^2\right)^{1/2} (x + h)\right],\ x \leq -h, \end{aligned} \tag{2}$$

and the corresponding TM magnetic fields, $H_y^{(i)}$, become,

$$\begin{aligned} H_y^{(3)} &= C \exp\left[-k\left(N^2 - n_3^2\right)^{1/2} x\right],\ x \geq 0, \\ H_y^{(1)} &= C \cos\left[k\left(n_1^2 - N^2\right)^{1/2} x\right] + D \sin\left[k(n_1^2 - N^2)^{1/2} x\right] \\ &\quad 0 \geq x \geq -h, \\ H_y^{(2)} &= \left\{C \cos\left[k\left(n_1^2 - N^2\right)^{1/2} h\right] - D \sin\left[k(n_1^2 - N^2)^{1/2} h\right]\right\} \\ &\quad \times \exp\left[k\left(N^2 - n_2^2\right)^{1/2} (x + h)\right],\ -h \geq x, \end{aligned} \tag{3}$$

where

$$n_i = c(\mu_i \varepsilon_i)^{1/2},\ i = 1,\ 2,\ 3, \tag{4}$$

denotes the corresponding real index of refraction. The TE mode amplitudes A and B pertain to electric fields in the film, $E_y^{(1)}$, and the TM mode amplitudes C and D pertain to magnetic fields in the film, $H_y^{(1)}$. The guided modes can exist provided $n_1 > n_2$ and $n_1 > n_3$. Conventionally, $n_3 \leq n_2$. Then $n_2 < N < n_1$ [10].

2.2. Guided TE and TM modes

The condition of continuity at the interfaces $x = 0$ and $x = -h$ of the **E** and **H** field components parallel to the interfaces provides the characteristic equations for the guided TE and TM modes, respectively [10, 12, 13],

$$\begin{aligned} kh\sqrt{n_1^2 - N^{(\mathrm{TE})2}} - \nu\pi &= \tan^{-1}\left(\frac{\mu_1}{\mu_2}\sqrt{\frac{N^{(\mathrm{TE})2} - n_2^2}{n_1^2 - N^{(\mathrm{TE})2}}}\right) \\ &\quad + \tan^{-1}\left(\frac{\mu_1}{\mu_3}\sqrt{\frac{N^{(\mathrm{TE})2} - n_3^2}{n_1^2 - N^{(\mathrm{TE})2}}}\right) \\ kh\sqrt{n_1^2 - N^{(\mathrm{TM})2}} - \nu\pi &= \tan^{-1}\left(\frac{\varepsilon_1}{\varepsilon_2}\sqrt{\frac{N^{(\mathrm{TM})2} - n_2^2}{n_1^2 - N^{(\mathrm{TM})2}}}\right) \\ &\quad + \tan^{-1}\left(\frac{\varepsilon_1}{\varepsilon_3}\sqrt{\frac{N^{(\mathrm{TM})2} - n_3^2}{n_1^2 - N^{(\mathrm{TM})2}}}\right). \end{aligned} \tag{5}$$

Their solutions provide an effective guide index, either $N^{(\mathrm{TE})}$ for TE modes or $N^{(\mathrm{TM})}$ for TM modes. $N^{(\mathrm{TE})}$ and $N^{(\mathrm{TM})}$ depend on the mode order, $\nu = 0, 1, 2, 3, \ldots$. The fundamental modes with $\nu = 0$ correspond to the maximal values of $N^{(\mathrm{TE})}$ and $N^{(\mathrm{TM})}$.

2.3. Goos–Hänchen shift and effective guide thickness

The lateral shift of the ray internally reflected at total reflection at a planar dielectric interface is known as the Goos–Hänchen shift [10]. In planar waveguides, the shifts occur at both interfaces. They must be considered separately for TE and TM polarizations. The half distances between the incident and reflected ray are denoted as $z_2^{(\mathrm{TE})}$ and $z_2^{(\mathrm{TM})}$ for the rays reflected at the interface between the film (1) and the substrate (2) and $z_3^{(\mathrm{TE})}$ and $z_3^{(\mathrm{TM})}$ for the rays reflected at the interface between the film (1) and the cover (3),

$$\begin{aligned} kz_2^{(\mathrm{TE})} &= \frac{\left(n_1^2 - N^{(\mathrm{TE})2}\right) + \left(N^{(\mathrm{TE})2} - n_2^2\right)}{\frac{\mu_2}{\mu_1}\left(n_1^2 - N^{(\mathrm{TE})2}\right) + \frac{\mu_1}{\mu_2}\left(N^{(\mathrm{TE})2} - n_2^2\right)} \\ &\quad \times \frac{N^{(\mathrm{TE})}}{\left(N^{(\mathrm{TE})2} - n_2^2\right)^{1/2}\left(n_1^2 - N^{(\mathrm{TE})2}\right)^{1/2}}, \end{aligned} \tag{6}$$

$$\begin{aligned} kz_3^{(\mathrm{TE})} &= \frac{\left(n_1^2 - N^{(\mathrm{TE})2}\right) + \left(N^{(\mathrm{TE})2} - n_3^2\right)}{\frac{\mu_3}{\mu_1}\left(n_1^2 - N^{(\mathrm{TE})2}\right) + \frac{\mu_1}{\mu_3}\left(N^{(\mathrm{TE})2} - n_3^2\right)} \\ &\quad \times \frac{N^{(\mathrm{TE})}}{\left(N^{(\mathrm{TE})2} - n_3^2\right)^{1/2}\left(n_1^2 - N^{(\mathrm{TE})2}\right)^{1/2}}, \end{aligned} \tag{7}$$

$$\begin{aligned} kz_2^{(\mathrm{TM})} &= \frac{\left(n_1^2 - N^{(\mathrm{TM})2}\right) + \left(N^{(\mathrm{TM})2} - n_2^2\right)}{\frac{\varepsilon_2}{\varepsilon_1}\left(n_1^2 - N^{(\mathrm{TM})2}\right) + \frac{\varepsilon_1}{\varepsilon_2}\left(N^{(\mathrm{TM})2} - n_2^2\right)} \\ &\quad \times \frac{N^{(\mathrm{TM})}}{\left(N^{(\mathrm{TM})2} - n_2^2\right)^{1/2}\left(n_1^2 - N^{(\mathrm{TM})2}\right)^{1/2}}, \end{aligned} \tag{8}$$

$$kz_3^{(\mathrm{TM})} = \frac{\left(n_1^2 - N^{(\mathrm{TM})2}\right) + \left(N^{(\mathrm{TM})2} - n_3^2\right)}{\frac{\varepsilon_3}{\varepsilon_1}\left(n_1^2 - N^{(\mathrm{TM})2}\right) + \frac{\varepsilon_1}{\varepsilon_3}\left(N^{(\mathrm{TM})2} - n_3^2\right)} \times \frac{N^{(\mathrm{TM})}}{\left(N^{(\mathrm{TM})2} - n_3^2\right)^{1/2}\left(n_1^2 - N^{(\mathrm{TM})2}\right)^{1/2}}, \tag{9}$$

The lateral half–shifts are related to the penetration depths, $x_2^{(\mathrm{TE})}$, $x_2^{(\mathrm{TM})}$, $x_3^{(\mathrm{TE})}$, and $x_3^{(\mathrm{TM})}$,

$$\tan\theta^{(\mathrm{TE})} = \frac{N^{(\mathrm{TE})}}{\left(n_1^2 - N^{(\mathrm{TE})2}\right)^{1/2}} = \frac{z_2^{(\mathrm{TE})}}{x_2^{(\mathrm{TE})}} = \frac{z_3^{(\mathrm{TE})}}{x_3^{(\mathrm{TE})}}, \tag{10}$$

$$\tan\theta^{(\mathrm{TM})} = \frac{N^{(\mathrm{TM})}}{\left(n_1^2 - N^{(\mathrm{TM})2}\right)^{1/2}} = \frac{z_2^{(\mathrm{TM})}}{x_2^{(\mathrm{TM})}} = \frac{z_3^{(\mathrm{TM})}}{x_3^{(\mathrm{TM})}}. \tag{11}$$

Here, $N^{(\mathrm{TE})}$ and $N^{(\mathrm{TM})}$ are the solutions of Equation (5) for TE and TM modes, respectively. The ratios in Equations (10) and (11) were expressed using the zig–zag angles, $\theta^{(\mathrm{TE})}$ and $\theta^{(\mathrm{TM})}$, of guided modes in the ray model [10].

The penetration depths, $x_2^{(\mathrm{TE})}$, $x_3^{(\mathrm{TE})}$, $x_2^{(\mathrm{TM})}$, and $x_3^{(\mathrm{TM})}$, follow from,

$$\begin{aligned} kx_2^{(\mathrm{TE})} &= \frac{\left(n_1^2 - N^{(\mathrm{TE})2}\right) + \left(N^{(\mathrm{TE})2} - n_2^2\right)}{\frac{\mu_2}{\mu_1}\left(n_1^2 - N^{(\mathrm{TE})2}\right) + \frac{\mu_1}{\mu_2}\left(N^{(\mathrm{TE})2} - n_2^2\right)} \frac{1}{\left(N^{(\mathrm{TE})2} - n_2^2\right)^{1/2}}, \\ kx_3^{(\mathrm{TE})} &= \frac{\left(n_1^2 - N^{(\mathrm{TE})2}\right) + \left(N^{(\mathrm{TE})2} - n_3^2\right)}{\frac{\mu_3}{\mu_1}\left(n_1^2 - N^{(\mathrm{TE})2}\right) + \frac{\mu_1}{\mu_3}\left(N^{(\mathrm{TE})2} - n_3^2\right)} \frac{1}{\left(N^{(\mathrm{TE})2} - n_3^2\right)^{1/2}}. \end{aligned} \tag{12}$$

$$\begin{aligned} kx_2^{(\mathrm{TM})} &= \frac{\left(n_1^2 - N^{(\mathrm{TM})2}\right) + \left(N^{(\mathrm{TM})2} - n_2^2\right)}{\frac{\varepsilon_2}{\varepsilon_1}\left(n_1^2 - N^{(\mathrm{TM})2}\right) + \frac{\varepsilon_1}{\varepsilon_2}\left(N^{(\mathrm{TM})2} - n_2^2\right)} \frac{1}{\left(N^{(\mathrm{TM})2} - n_2^2\right)^{1/2}}, \\ kx_3^{(\mathrm{TM})} &= \frac{\left(n_1^2 - N^{(\mathrm{TM})2}\right) + \left(N^{(\mathrm{TM})2} - n_3^2\right)}{\frac{\varepsilon_3}{\varepsilon_1}\left(n_1^2 - N^{(\mathrm{TM})2}\right) + \frac{\varepsilon_1}{\varepsilon_3}\left(N^{(\mathrm{TM})2} - n_3^2\right)} \frac{1}{\left(N^{(\mathrm{TM})2} - n_3^2\right)^{1/2}}. \end{aligned} \tag{13}$$

The effective guide thickness, h_{eff}, is defined as a sum of the film thickness, h, and the penetration depths into the substrate, x_2, and the cover, x_3, separately for TE and TM modes.

$$h_{\mathrm{eff}}^{(\mathrm{TE})} = h + x_2^{(\mathrm{TE})} + x_3^{(\mathrm{TE})}, \; h_{\mathrm{eff}}^{(\mathrm{TM})} = h + x_2^{(\mathrm{TM})} + x_3^{(\mathrm{TM})}. \tag{14}$$

2.4. Power carried by TE and TM modes

The time-averaged power carried by the TE and TM modes in the waveguide parallel to the z axis across the area in the xy plane bounded by $-\infty < x < \infty$, and $-1/2 < y < 1/2$ follows from [13],

$$\begin{aligned} P^{(\mathrm{TE})} &= \frac{N^{(\mathrm{TE})}}{2c}\left[\frac{1}{\mu_3}\int_{-\infty}^{-h} |E_y|^2 \mathrm{d}x \right. \\ &\quad \left. + \frac{1}{\mu_1}\int_{-h}^{0} |\mathrm{E}_y|^2 \mathrm{d}x + \frac{1}{\mu_2}\int_{0}^{\infty} |E_y|^2 \mathrm{d}x, \right. \\ P^{(\mathrm{TM})} &= \frac{N^{(\mathrm{TM})}}{2c}\left[\frac{1}{\varepsilon_3}\int_{-\infty}^{-h} |H_y|^2 \mathrm{d}x + \frac{1}{\varepsilon_1}\int_{-h}^{0} |H_y|^2 \mathrm{d}x \right. \\ &\quad \left. + \frac{1}{\varepsilon_2}\int_{0}^{\infty} |H_y|^2 \mathrm{d}x. \right. \end{aligned} \tag{15}$$

The substitutions according to Equations (2) and (3) and the account of Equations (1) and (5) provide,

$$\begin{aligned} P^{(\mathrm{TE})} &= \frac{N^{(\mathrm{TE})}\left(|A|^2 + |B|^2\right)}{4c\mu_1} h_{\mathrm{eff}}^{(\mathrm{TE})}, \\ P^{(\mathrm{TM})} &= \frac{N^{(\mathrm{TM})}\left(|C|^2 + |D|^2\right)}{4c\varepsilon_1} h_{\mathrm{eff}}^{(\mathrm{TM})}. \end{aligned} \tag{16}$$

where $h_{\mathrm{eff}}^{(\mathrm{TE})}$ and $h_{\mathrm{eff}}^{(\mathrm{TM})}$ are given by Equation (14).

2.5. Normalized characteristics

The characteristic equations can be transformed into a normalized form using three parameters, that is, the normalized kh product, V, normalized guide index, b, and asymmetry measure, a, defined as [5],

$$\begin{aligned} V &= hk\left(n_1^2 - n_2^2\right)^{1/2}, 0 < V < \infty, \\ b &= \frac{N^2 - n_2^2}{n_1^2 - n_2^2}, \; 0 < b < 1, \\ a &= \frac{n_2^2 - n_3^2}{n_1^2 - n_2^2}, \; 0 \le a < \infty. \end{aligned} \tag{17}$$

The normalized characteristic equations for TE and TM modes become, respectively [9],

$$\begin{aligned} V^{(\mathrm{TE})}\left(1 - b^{(\mathrm{TE})}\right)^{1/2} - \nu\pi &= \tan^{-1}\left[\frac{\mu_1}{\mu_2}\left(\frac{b^{(\mathrm{TE})}}{1 - b^{(\mathrm{TE})}}\right)^{1/2}\right] \\ &\quad + \tan^{-1}\left[\frac{\mu_1}{\mu_3}\left(\frac{b^{(\mathrm{TE})} + a}{1 - b^{(\mathrm{TE})}}\right)^{1/2}\right], \\ V^{(\mathrm{TM})}\left(1 - b^{(\mathrm{TM})}\right)^{1/2} - \nu\pi &= \tan^{-1}\left[\frac{\varepsilon_1}{\varepsilon_2}\left(\frac{b^{(\mathrm{TM})}}{1 - b^{(\mathrm{TM})}}\right)^{1/2}\right] \\ &\quad + \tan^{-1}\left[\frac{\varepsilon_1}{\varepsilon_3}\left(\frac{b^{(\mathrm{TM})} + a}{1 - b^{(\mathrm{TM})}}\right)^{1/2}\right]. \end{aligned} \tag{18}$$

The normalized cutoff V for the fundamental modes ($\nu = 0$) follows from the condition $b \to 0$ [10],

$$V_{\mathrm{cutoff}}^{(\mathrm{TE})} = \tan^{-1}\left(\frac{\mu_1}{\mu_3} a^{1/2}\right), \; V_{\mathrm{cutoff}}^{(\mathrm{TM})} = \tan^{-1}\left(\frac{\varepsilon_1}{\varepsilon_3} a^{1/2}\right). \tag{19}$$

Note that the expression, $(\varepsilon_1/\varepsilon_3)^2 a$, corresponds to the asymmetry measure for the TM modes defined by Kogelnik and Ramaswamy [5].

Normalized effective guide thickness is defined by [10],

$$\mathscr{H}^{(\mathrm{TE})} = kh_{\mathrm{eff}}^{(\mathrm{TE})}\left(n_1^2 - n_2^2\right)^{1/2}, \; \mathscr{H}^{(\mathrm{TM})} = kh_{\mathrm{eff}}^{(\mathrm{TM})}\left(n_1^2 - n_2^2\right)^{1/2}. \tag{20}$$

and can be expressed as a function of V,

$$\begin{aligned} \mathscr{H}^{(\mathrm{TE})} &= V^{(\mathrm{TE})} + \mathscr{X}_2^{(\mathrm{TE})} + \mathscr{X}_3^{(\mathrm{TE})}, \\ \mathscr{H}^{(\mathrm{TM})} &= V^{(\mathrm{TM})} + \mathscr{X}_2^{(\mathrm{TM})} + \mathscr{X}_3^{(\mathrm{TM})}. \end{aligned} \tag{21}$$

and the normalized penetration depths,

$$\begin{aligned}\mathscr{X}_2^{(\mathrm{TE})} &= k\left(n_1^2-n_2^2\right)^{1/2} x_2^{(\mathrm{TE})} \\ &= \frac{1}{\frac{\mu_2}{\mu_1}\left(1-b^{(\mathrm{TE})}\right)+\frac{\mu_1}{\mu_2}b^{(\mathrm{TE})}}\ \frac{1}{b^{(\mathrm{TE})1/2}}, \\ \mathscr{X}_3^{(\mathrm{TE})} &= k\left(n_1^2-n_2^2\right)^{1/2} x_3^{(\mathrm{TE})} \\ &= \frac{1+a}{\frac{\mu_3}{\mu_1}\left(1-b^{(\mathrm{TE})}\right)+\frac{\mu_1}{\mu_3}\left(b^{(\mathrm{TE})}+a\right)}\ \frac{1}{\left(b^{(\mathrm{TE})}+a\right)^{1/2}},\end{aligned} \tag{22}$$

$$\begin{aligned}\mathscr{X}_2^{(\mathrm{TM})} &= k\left(n_1^2-n_2^2\right)^{1/2} x_2^{(\mathrm{TM})} \\ &= \frac{1}{\frac{\varepsilon_2}{\varepsilon_1}\left(1-b^{(\mathrm{TM})}\right)+\frac{\varepsilon_1}{\varepsilon_2}b^{(\mathrm{TM})}}\ \frac{1}{b^{(\mathrm{TM})1/2}}, \\ \mathscr{X}_3^{(\mathrm{TM})} &= k\left(n_1^2-n_2^2\right)^{1/2} x_3^{(\mathrm{TM})} \\ &= \frac{1+a}{\frac{\varepsilon_3}{\varepsilon_1}\left(1-b^{(\mathrm{TM})}\right)+\frac{\varepsilon_1}{\varepsilon_3}\left(b^{(\mathrm{TM})}+a\right)}\ \frac{1}{\left(b^{(\mathrm{TM})}+a\right)^{1/2}}.\end{aligned} \tag{23}$$

The asymptotes to $\mathscr{H}^{(\mathrm{TE})}(V)$ and $\mathscr{H}^{(\mathrm{TM})}(V)$ far from the cutoff are found from Equation (21) using Equations (22) and (23),

$$\begin{aligned}\lim_{b\to 1}\mathscr{H}^{(\mathrm{TE})} &= V^{(\mathrm{TE})}+\frac{\mu_2}{\mu_1}+\frac{\mu_3}{\mu_1}(1+a)^{-1/2}, \\ \lim_{b\to 1}\mathscr{H}^{(\mathrm{TM})} &= V^{(\mathrm{TM})}+\frac{\varepsilon_2}{\varepsilon_1}+\frac{\varepsilon_3}{\varepsilon_1}(1+a)^{-1/2}.\end{aligned} \tag{24}$$

In the following, Equations (18) and (21) will be applied to compute the charts of $b(V)$ and $\mathscr{H}(V)$ with the restriction to the cases where the magnetic permeabilities in the film, substrate, and cover reduce to the vacuum value with $\mu_1/\mu_2 = \mu_1/\mu_3 = 1$. The considered illustrations involve the cases of $n_1/n_2 = 1.015$, $n_1/n_2 = 1.15$, and $n_1/n_2 = 1.5$, with a confined to the practical ranges of asymmetry measure, $a \le 30$, $a \le 2.8$, and $a \le 0.5$, respectively.

Figure 2
Normalized effective guide index, b, as a function of V for fundamental TE and TM modes ($\nu = 0$) in asymmetric waveguides. (see Table 1)

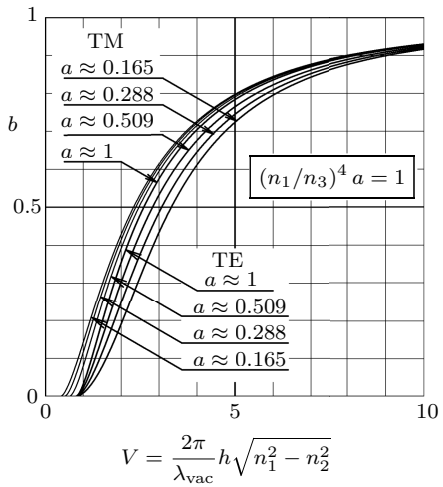

Figure 3
Normalized effective guide index, b, as a function of V for TM modes of the order $\nu = 0$, 1, 2, and 3 in the waveguides characterized by the ratio of refractive indices of the film (n_1) and the substrate (n_2) $n_1/n_2 = 1.015$, and the asymmetry measure a, for $a = 0$, 1, 30. Dashed curves indicate the corresponding TE modes with $a = 30$ (see Table 2)

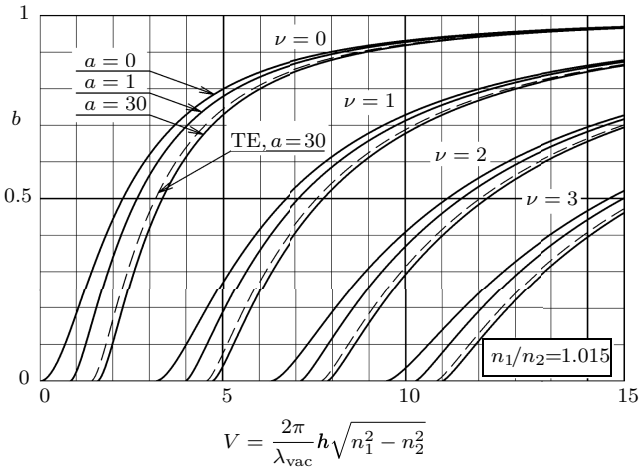

Figure 4
Normalized effective guide index, b, as a function of V for fundamental TM modes in the waveguides characterized by the ratio of refractive indices of the film (n_1) and the substrate (n_2), $n_1/n_2 = 1.015$ and by the asymmetry measure a for $a = 0$, 0.2, 0.5, 1, 2, 5, 10, 30 (see Table 2)

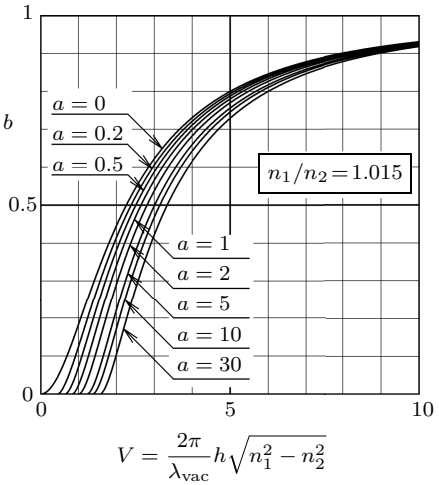

3. Normalized Effective Guide Index

Figures 2–8 display $b(V)$ computed with Equation (18). The relevant parameters are summarized in Tables 1–4. Figure 2 shows the fundamental TM modes with the same $V_{\mathrm{cutoff}}^{(\mathrm{TM})}$ compared with the fundamental TE modes characterized by the same n_1/n_2 and a. The parameters for this case are collected in Table 1 and correspond to those considered by Kogelnik and Ramaswamy in Figure 5 [5]. Table 2 and Figures 3 and 4 illustrate the case of

Figure 5
Normalized effective guide index, b, as a function of V for TM modes of the order ν = 0, 1, and 2 in the waveguides characterized by the ratio of refractive indices of the film (n_1) and the substrate (n_2), n_1/n_2 = 1.15 and by the asymmetry measure a for a = 0, 0.5, 2.8. Dashed curves represent TE modes with a = 2.8 (see Table 3)

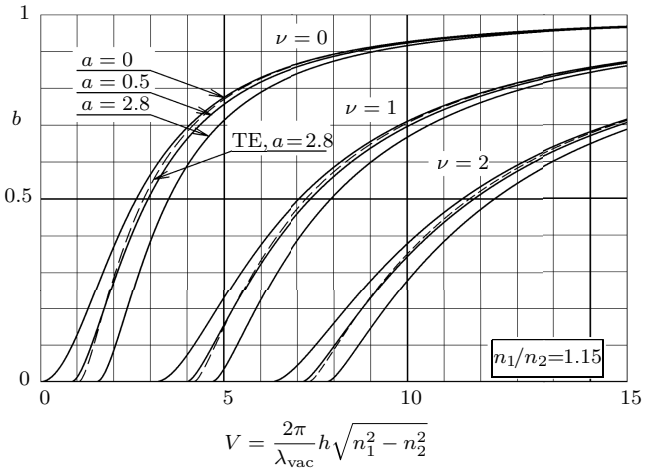

Figure 6
Normalized effective guide index, b, as a function of V for fundamental TM modes in the waveguides characterized by the ratio of refractive indices of the film (n_1) and the substrate (n_2), n_1/n_2 = 1.15 and by the asymmetry measure a for a = 0, 0.2, 0.5, 1, 1.5, 2, 2.8 (see Table 3)

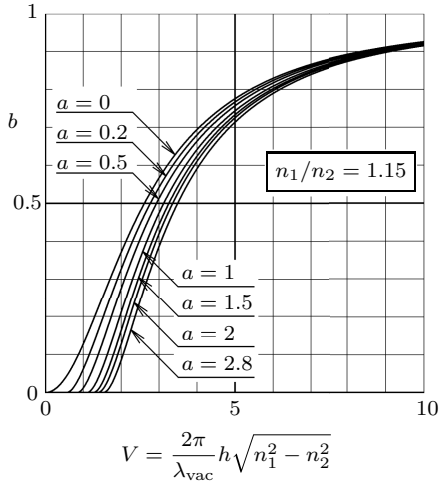

n_1/n_2 = 1.015. Because of (n_1/n_2) close to one, appreciable differences between TE and TM modes of the order ν = 0, 1, 2, 3 take place only at higher a, as shown in Figure 3 for a = 30. Figure 4 displays $b(V)$ for the fundamental TM modes at several a, $0 \le a \le 30$. The data for n_1/n_2 = 1.15 of Table 3 were employed in the construction of Figure 5, showing $b(V)$ for TM modes of ν = 0, 1, 2 and a = 0, 0.5, 2.8. Figure 5 illustrates the difference in $b(V)$ between TE and TM modes for the highest asymmetry measure, a = 2.8. The family of $b(V)$ curves for the fundamental TM modes of $0 \le a \le 2.8$ is plotted in Figure 6. The differences between the TE and TM modes become even more important for the case of the highest considered ratio, n_1/n_2 = 1.5. The relevant data are collected in Table 4 and employed in Figures 7 and 8.

Figure 7
Normalized effective guide index, b, as a function V of for TM modes of the order ν = 0, 1, 2, and 3 in the waveguides characterized by the ratio of refractive indices of the film (n_1) and the substrate (n_2), n_1/n_2 = 1.5 and by the asymmetry measure a for a = 0, 0.2, and 0.5. Dashed curves represent TE modes with a = 0.5 (see Table 4)

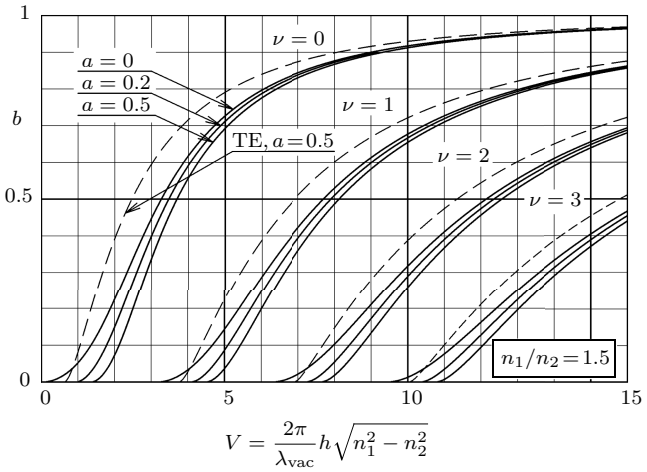

Figure 8
Normalized effective guide index, b, as a function of V for the fundamental TE and TM modes (ν = 0) in the waveguides characterized by the ratio of refractive indices of the film (n_1) and the substrate (n_2), n_1/n_2 = 1.5 and by the asymmetry measure a for a = 0, 0.2, and 0.5 (see Table 4)

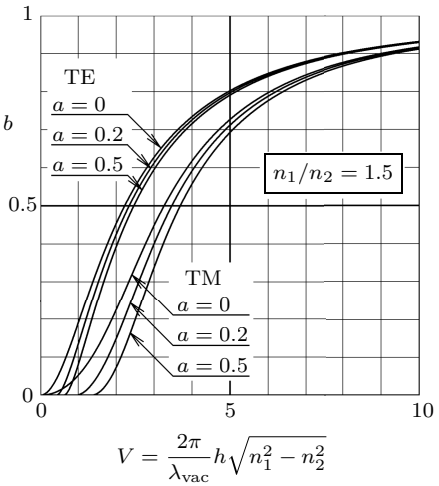

4. Normalized Effective Guide Thickness

The evaluation of the normalized effective guide thickness employs Equation (21). For fixed a of 0 and 0.5, Figures 9 and 10 illustrate the effect of n_1/n_2 on $\mathscr{H}(V)$ for the TM modes (Table 5). The minimum of $\mathscr{H}_{\min}^{(\mathrm{TM})}(V)$ at a = 0 shifts to a higher V as n_1/n_2 increases with respect to the corresponding minimum of the TE modes, that is, $\mathscr{H}_{\min}^{(\mathrm{TE})}(1.73)$ = 4.93 [5]. For a = 0, the value of $\mathscr{H}_{\min}^{(\mathrm{TM})}(V)$ increases with n_1/n_2 up to $n_1/n_2 \approx 1.3$ ($\mathscr{H}_{\min}^{(\mathrm{TM})}(2.83) \approx 5.41$) where it starts to decrease. For a = 0.5, the

Table 1
TE and TM modes in asymmetric waveguides

n_1/n_2	n_1/n_3	a	$(n_1/n_3)^4 a$	$V_{\text{cutoff}}^{(\text{TE})}$	$V_{\text{cutoff}}^{(\text{TM})}$
≈1	≈1	≈1	1	0.7852	0.7854
$0.9^{-1} \approx 1.1111$	1.1840	0.5088	1	0.6196	0.7854
$0.8^{-1} = 1.25$	1.3654	0.28774	1	0.4924	0.7854
$0.7^{-1} \approx 1.4286$	1.5695	0.1648	1	0.3856	0.7854

Table 2
TE and TM modes in waveguides characterized by the ratio of refractive indices of the film (n_1) and the substrate (n_2), n_1/n_2 = 1.015

n_1/n_2	n_1/n_3	a	$(n_1/n_3)^4 a$	$V_{\text{cutoff}}^{(\text{TE})}$	$V_{\text{cutoff}}^{(\text{TM})}$
1.015	1.015	0	0	0	0
1.015	1.01808	0.2	0.214863	0.420535	0.434051
1.015	1.02276	0.5	0.547093	0.61548	0.636849
1.015	1.0307	1	1.12855	0.785398	0.815614
1.015	1.0471	2	2.40467	0.955317	0.998036
1.015	1.1017	5	7.36456	1.15026	1.21774
1.015	1.21511	10	21.8002	1.26452	1.35981
1.015	3.32385	30	3661.73	1.39021	1.55427

Table 3
TE and TM modes in the waveguides characterized by the ratio of refractive indices of the film (n_1) and the substrate (n_2), n_1/n_2 = 1.15

n_1/n_2	n_1/n_3	a	$(n_1/n_3)^4 a$	$V_{\text{cutoff}}^{(\text{TE})}$	$V_{\text{cutoff}}^{(\text{TM})}$
1.15	1.15	0	0	0	0
1.15	1.25569	0.5	1.24307	0.61548	0.839688
1.15	1.397152	1	3.8105	0.785398	1.0974
1.15	1.6005	1.5	9.8438	0.886077	1.26225
1.15	1.93012	2	27.7567	0.955317	1.38322
1.15	2.19546	2.25	52.2739	0.982794	1.43336
1.15	3.6924	2.8	520.466	1.03213	1.52699

Table 4
TE and TM modes in the waveguides characterized by the ratio of refractive indices of the film (n_1) and the substrate (n_2), n_1/n_2 = 1.5

n_1/n_2	n_1/n_3	a	$(n_1/n_3)^4 a$	$V_{\text{cutoff}}^{(\text{TE})}$	$V_{\text{cutoff}}^{(\text{TM})}$
1.5	1.5	0	0	0	0
1.5	1.7321	0.2	1.8	0.4205	0.9303
1.5	2.44949	0.5	18	0.61548	1.3393

Figure 9
Normalized effective guide thickness, $\mathscr{H}$, as a function of V for the fundamental TE (dashed) and TM modes in the symmetric waveguides characterized by the ratios of refractive indices of the film (n_1) and the substrate (n_2), n_1/n_2 = 1.05, 1.15, 1.2, 1.3 and 1.5. The dash dotted line represents the asymptote to $\mathscr{H}$ far from the cutoff for the TM mode with n_1/n_2 = 1.5 (see Table 5)

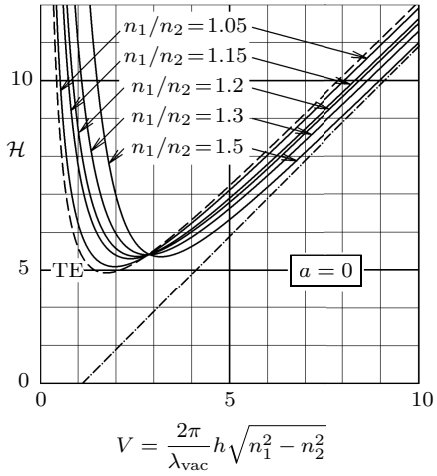

Figure 10
Normalized effective guide thickness, $\mathscr{H}$, as a function of V for the fundamental TE (dashed) and TM modes characterized by the ratios of refractive indices of the film (n_1) and the substrate ($n2$), n_1/n_2 = 1.05, 1.15, 1.2, 1.3 and 1.5 and by the asymmetry measure a = 0.5. The dash dotted line represents the asymptote to $\mathscr{H}$ far from the cutoff for the TM mode with n_1/n_2 = 1.5 (see Table 5)

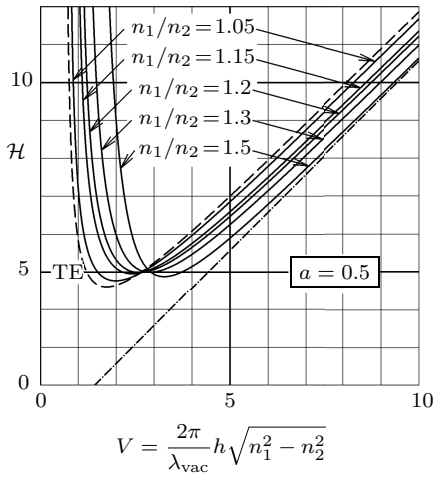

Figure 11
Normalized effective guide thickness, $\mathscr{H}$ as a function of V for TM fundamental modes (v = 0) in the waveguides characterized by the ratio of refractive indices of the film (n_1) and the substrate (n_2), n_1/n_2 = 1.015, and the asymmetry measure, a. The dash dotted line represents the asymptote to $\mathscr{H}$ far from the cutoff for the TM mode with a = 30 (see Table 2)

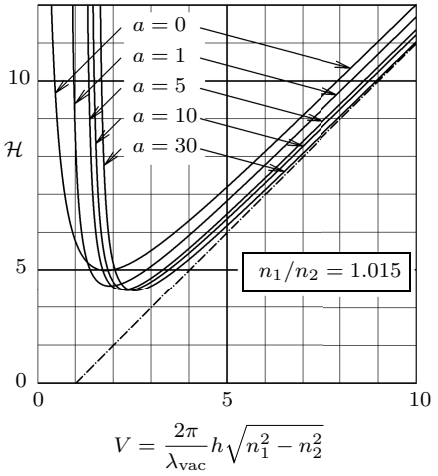

Figure 12
Normalized effective guide thickness as a function of V for TE (dashed) and TM fundamental modes (v = 0) in the waveguides characterized by the ratio of refractive indices of the film (n_1) and the substrate (n_2), n_1/n_2 = 1.015, and by the asymmetry measure a, a = 0, 1 and 30. The dash dotted line represents the asymptote to $\mathscr{H}$ far from the cutoff for the TM mode with a = 30 (see Table 2)

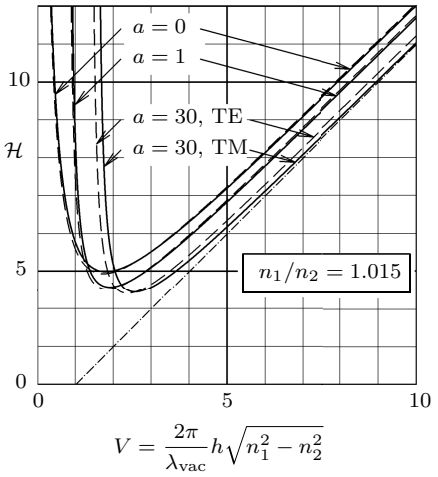

behavior is similar, $\mathscr{H}_{min}^{(TM)}(V)$ increases with n_1/n_2 up to $n_1/n_2 \approx 1.25$ ($\mathscr{H}_{min}^{(TM)}(2.78) \approx 5.01$).

Figure 11 shows $\mathscr{H}(V)$ of the fundamental TM modes with $0 \leq a \leq 30$ for $n_1/n_2 = 1.015$. The behavior is compared with that of the TE modes in Figure 12. The trends are in both TE and TM cases the same, that is., the minimum of $\mathscr{H}(V)$ shifts to higher V with a and becomes deeper. At $a = 30$, the minimum $\mathscr{H}_{min}^{(TM)}(2.63) \approx 4.44$ is only slightly translated with respect to the minimum $\mathscr{H}_{min}^{(TE)}(2.59) \approx 4.44$. At lower a, the differences between $\mathscr{H}(V)^{(TE)}$ and $\mathscr{H}(V)^{(TM)}$ are seen to be even less important [5].

Figure 13 shows $\mathscr{H}(V)^{(TM)}$ at $n_1/n_2 = 1.15$. The situations for the TM a TE modes now significantly depart from each other (Figure 14). The minima for $a = 2.8$ differ both in the positions

Figure 13
Normalized effective guide thickness, $\mathscr{H}$ as a function of V for TM fundamental modes (v = 0) in the waveguides characterized by the ratio of refractive indices of the film (n_1) and the substrate (n_2), n_1/n_2 = 1.15, and by the asymmetry measure a. The dash dotted line represents the asymptote to $\mathscr{H}$ far from the cutoff for the TM mode with a = 30 (see Table 3)

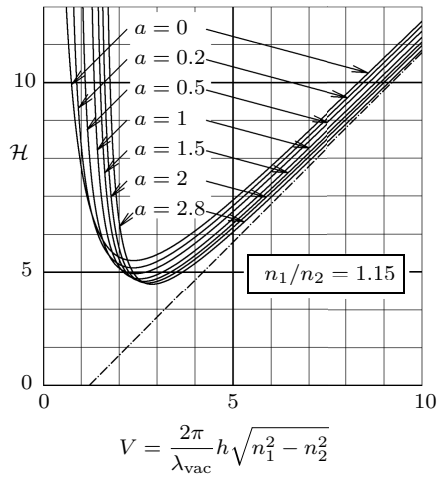

Figure 14
Normalized effective guide thickness as a function of V for TE (dashed) and TM fundamental modes (v = 0) in the waveguides characterized by the ratio of refractive indices of the film (n_1) and the substrate (n_2), n_1/n_2 = 1.15, and by the asymmetry measure a, for a = 0, 0.5, and 2.8. The dash dotted line represents the asymptote to $\mathscr{H}$ far from the cutoff for the TM mode with a = 30 (see Table 3)

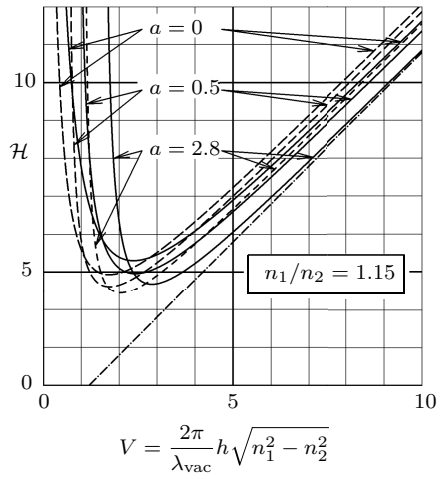

and in the magnitudes as can be seen from the comparison of $\mathscr{H}_{\min}^{(\mathrm{TE})}(2.04) \approx 4.43$ and $\mathscr{H}_{\min}^{(\mathrm{TM})}(2.86) \approx 4.68$. The separation of $\mathscr{H}(V)^{(\mathrm{TE})}$ and $\mathscr{H}(V)^{(\mathrm{TM})}$ is the biggest in the last considered case of $n_1/n_2 = 1.5$ given in Figure 15, where for $a = 0$, $\mathscr{H}_{\min}^{(\mathrm{TE})}(1.73) \approx 4.93$ and $\mathscr{H}_{\min}^{(\mathrm{TM})}(3.21) \approx 5.36$, while for $a = 0.5$, $\mathscr{H}_{\min}^{(\mathrm{TE})}(1.74) \approx 4.61$ and $\mathscr{H}_{\min}^{(\mathrm{TM})}(3.28) \approx 4.88$.

Figure 15
Normalized effective guide thickness as a function of V for the fundamental TE and TM in the waveguides characterized by the ratio of refractive indices of the film (n_1) and the substrate (n_2), n_1/n_2 = 1.5, and by the asymmetry measure a, for a = 0, 0.2 and 0.5. The dash dotted line represents the asymptote to $\mathscr{H}$ far from the cutoff for the TM mode with a = 0.5 (see Table 4)

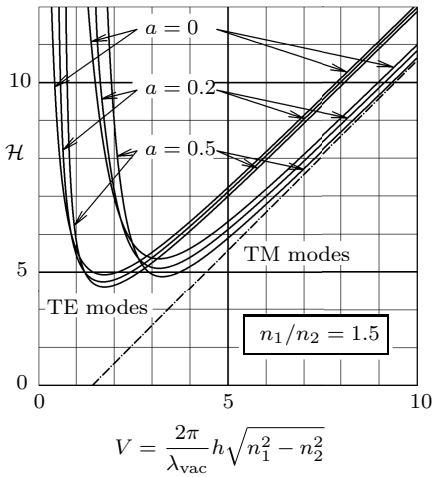

Table 5
TE and TM modes for the asymmetry measure a = 0 and 0.5

n_1/n_2	n_1/n_3	a	$(n_1/n_3)^4\, a$	$V_{\mathrm{cutoff}}^{(\mathrm{TE})}$	$V_{\mathrm{cutoff}}^{(\mathrm{TM})}$
1.05	1.05	0	0	0	0
1.05	1.07799	0.5	0.675186	0.61548	0.687832
1.15	1.15	0	0	0	0
1.15	1.2557	0.5	1.24307	0.61548	0.8397
1.2	1.2	0	0	0	0
1.2	1.35873	0.5	1.70414	0.61548	0.917114
1.3	1.3	0	0	0	0
1.3	1.60629	0.5	3.32859	0.61548	1.0694
1.5	1.5	0	0	0	0
1.5	2.44949	0.5	18	0.61548	1.3393

5. Conclusion

This paper provided the analysis of TE and TM waveguide modes in asymmetric planar structures consisting of three linear isotropic dielectric regions, a film, a substrate, and a cover (slab optical waveguide). TE and TM mode characteristics were related by symmetry. The corresponding equations written in concise and consistent forms provided the guide index, N, the Goos–Hänchen shift, the effective guide thickness, h_{eff}, and the power, P, carried by the modes. The normalized guide index, b, and the normalized effective thickness, $\mathscr{H}$, as functions of the normalized frequency, V, in the realistic ranges of the asymmetry measure, a, were displayed in charts with the focus on TM modes. The purpose of the present treatment was to complement the scaling rules for TE modes by Kogelnik and Ramaswamy [5] with those for symmetry-related TM modes. To display all practical

situations in (non–magnetic) dielectric waveguides, the scaling rules for TM modes are required to account for the realistic range of the permittivity ratios, $\varepsilon_1/\varepsilon_2$ and $\varepsilon_1/\varepsilon_3$, with respect to those for TE modes, where the magnetic permeability ratios are reduced to unity, $\mu_1/\mu_2 \approx 1$ and $\mu_1/\mu_3 \approx 1$. To display either $b(V,a)$ or $\mathscr{H}(V,a)$, several charts were necessary for TM modes, whereas a single one was sufficient for TE modes. The use of the same variables, V and a, in the charts for b and $\mathscr{H}$ enabled to appreciate, among others, the differences between TE and TM modes in the cutoff regions of the modes. The positions of $\mathscr{H}$ minima, different for TE and TM modes, which correspond to maximal power confinement in the film, which is favorable for the generation of nonlinear optical effects, are evaluated both on the same scale as functions of V. In a more general way, thanks to the common independent variable V, the differences between TE and TM modes in the normalized guide index, $b(V)$, and the normalized effective thickness, $\mathscr{H}(V)$, which increase with the permittivity ratios, $\varepsilon_1/\varepsilon_2$ in the film (1) and the substrate (2) and with the asymmetry measure, a, are determined for physically the same waveguide. This basic optical waveguide configuration finds application in various optical waveguide devices. Its understanding will be useful in the analysis of multilayer optical waveguides, optical waveguides with smooth permittivity profiles, optical isolators and optical waveguide biosensors, etc., working in a wide range from terahertz to visible frequencies [11, 15–25].

Ethical Statement

This study does not contain any studies with human or animal subjects performed by the author.

Conflicts of Interest

The author declares that he has no conflicts of interest to this work.

Data Availability Statement

Data sharing is not applicable to this article as no new data were created or analyzed in this study.

Author Contribution Statement

Štefan Višňovský: Conceptualization, Methodology, Software, Validation, Formal analysis, Investigation, Writing - original draft, Writing - review & editing, Visualization, Supervision, Project administration.

References

[1] Wu, Y.-D. (2020). A general method for analyzing arbitrary planar negative-refractive-index multilayer slab optical waveguide structures. *Scientific Report*, *10*(1), 14964. https://doi.org/10.1038/s41598-020-72017-3

[2] Kanjwal, M. A., & Ghaferi, A. A. (2022). Advanced waveguide based LOC biosensors: A minireview. *Sensors*, *22*(14), 5443. https://doi.org/10.3390/s22145443

[3] Alwan, S. T., Al-Bawee, A., & Alrubaiy, A. (2024). Behavior of TE and TM propagation modes in nanomaterial graphene using asymmetric slab waveguide. *Curved and Layered Structures*, *11*(1), 20240021. https://doi.org/10.1515/cls-2024-0021

[4] Shen, L. F., Xie, J. P., & Wang, Z. H. (2021). Tunable TM modes in a slab waveguide including a graphene-dielectric multilayer structure. *Optik*, *227*, 165414. https://doi.org/10.1016/j.ijleo.2020.165414

[5] Kogelnik, H., & Ramaswamy, V. (1974). Scaling rules for thin–film optical waveguides. *Applied Optics*, *13*(8), 1857–1862. https://doi.org/10.1364/AO.13.001857

[6] Pershan, P. S. (1967). Magneto–optical effects. *Journal of Applied Physics*, *38*(3), 1482–1490. https://doi.org/10.1063/1.1709678

[7] Hewak, D. W., & Lit, J. W. Y. (1986). Generalized dispersion properties of thin–film waveguides. *Applied Optics*, *25*(12), 1977–1981. https://doi.org/10.1364/AO.25.001977

[8] Hewak, D. W., & Lit, J. W. Y. (1987). Normalized parameters for the guiding properties of TM modes in a thin–film waveguide. *Journal of the Optical Society of America A*, *4*(5), 847–850. https://doi.org/10.1364/JOSAA.4.000847

[9] Wang, Z. H., Xiao, Z. Y., & Li, S. P. (2008). Guided modes in slab waveguides with a left handed material cover or substrate. *Optics Communication*, *281*(4), 607–613. https://doi.org/10.1016/j.optcom.2007.10.034

[10] Kogelnik, H. (1975). Theory of dielectric waveguides. In T. Tamir (Ed.), *Integrated optics* (pp. 13–81). Springer. https://doi.org/10.1007/978-3-662-43208-2_2

[11] Yang, H. W., Dong, P., & Liu, Y. (2009). Transmission properties of asymmetric slab waveguides with left–handed materials. *Journal of Russian Laser Research*, *30*(2), 193–203. https://doi.org/10.1007/s10946-009-9060-7

[12] Marcuse, D. (1972). *Light transmission optics*. USA: Van Nostrand Reinhold Company.

[13] Marcuse, D. (1974). *Theory of dielectric optical waveguides*. USA: Academic Press.

[14] Tien, P. K. (1977). Integrated optics and new wave phenomena in optical waveguides. *Reviews of Modern Physics*, *49*(2), 361–420. https://doi.org/10.1103/REVMODPHYS.49.361

[15] Islamov, I., Bashirov, R., & Ismayilov, N. (2023). Modeling of a telecommunication optical waveguide with anisotropic medium. *International Journal of Microwave and Optical Technology*, *18*(5), 540–549.

[16] Broquin, J.-E., & Honkanen, S. (2021). Integrated photonics on glass: A review of the ion-exchange technology achievements. *Applied Sciences*, *11*(10), 4472. https://doi.org/10.3390/app11104472

[17] Wei, Z., Yang, Y., Wu, D., Wang, J., Ma, X., Zhao, X., . . . , & Bi, L. (2025). Recent development of magneto-optical thin films and integrated photonic devices. *Journal of Materials Chemistry C*, *13*(25), 12628–12649. https://doi.org/10.1039/D5TC01540E

[18] Teng, D., & Wang, K. (2021). Theoretical analysis of terahertz dielectric loaded graphene waveguide. *Nanomaterials*, *11*(1), 210. https://doi.org/10.3390/nano11010210

[19] Passarelli, N., Palomba, S., Kabakova, I., & de Sterke, C. M. (2024). Rational design of an integrated directional coupler for wideband operation. *Applied Optics*, *63*(14), D28–D34. https://doi.org/10.1364/AO.514816

[20] Chen, Y., Yang, Z., Wang, L., Dong, W., & Chen, Z. (2023). Chiral hybrid waveguide-plasmon resonances. *Optics Express*, *31*(4), 5927–5939. https://doi.org/10.1364/OE.482211

[21] Chen, J., & Rong, K. (2021). Nanophotonic devices and circuits based on colloidal quantum dots. *Materials Chemistry Frontiers*, *5*(12), 4502–4537. https://doi.org/10.1039/d0qm01118e

[22] Kumar Singh, A., & Huang, J.-S. (2022). Optical responses of Fano resonators in non-spectral parametric domains. *Optics Letters*, *47*(15), 3720–3723. https://doi.org/10.1364/OL.465901

[23] Khozeymeh, F., & Razaghi, M. (2021). Sensitivity and intrinsic limit of detection improvement in a photonic refractive-index sensor. *Optik*, *247*, 167844. https://doi.org/10.1016/j.ijleo.2021.167844

[24] Tuniz, A., Song, A. Y., Della Valle, G., & de Sterke, C. M. (2022). Plasmonic sensors beyond the phase matching condition: a simplified approach. *Sensors*, *22*(24), 9994. https://doi.org/10.3390/s22249994

[25] Roy, S., Mondal, S., & Debnath, K. (2023). Generation of tunable circular dichroism—Design and sensor applications. *IEEE Sensors Journal*, *23*(1), 285–292. https://doi.org/10.1109/JSEN.2022.3221437

How to Cite: Višňovský, Š. (2026). Scaling Rules for TM Modes in Thin–Film Optical Waveguides. *Journal of Optics and Photonics Research*. https://doi.org/10.47852/bonviewJOPR62027912